

Multilayer nanoparticle arrays for broad spectrum absorption enhancement in thin film solar cells

Aravind Krishnan,^{1,*} Snehal Das,¹ Siva Rama Krishna,¹ and Mohammed Zafar Ali Khan,¹

¹ Department of Electrical Engineering, Indian Institute of Technology Hyderabad, ODF Estate, Medak District, Andhra Pradesh-502205, India

*ee10b004@iith.ac.in

Abstract: In this paper, we present a theoretical study on the absorption efficiency enhancement of a thin film amorphous Silicon (a-Si) photovoltaic cell over a broad spectrum of wavelengths using multiple nanoparticle arrays. The light absorption efficiency is enhanced in the lower wavelengths by a nanoparticle array on the surface and in the higher wavelengths by another nanoparticle array embedded in the active region. The efficiency at intermediate wavelengths is enhanced by the constructive interference of plasmon coupled light. We optimize this design by tuning the radius of particles in both arrays, the period of the array and the distance between the two arrays. The optimization results in 61.44% increase in total quantum efficiency for a 0.5 μm thick a-Si substrate.

© 2018 Optical Society of America

OCIS codes: 250.5403; 240.6680; 230.0250; 310.6845; 350.6050; 290.4020.

References and links

1. H. A. Atwater and A. Polman, "Plasmonics for improved photovoltaic devices," *Nature Mater.* **9**, 205 (2010).
2. K. R. Catchpole and A. Polman, "Plasmonic solar cells," *Opt. Express* **16**, 21793 (2008).
3. Y. A. Akimov and W. S. Koh, "Design of Plasmonic Nanoparticles for Efficient Subwavelength Light Trapping in Thin-Film Solar Cells," *Plasmonics* **6**, 155 (2011).
4. S. Pillai, K. R. Catchpole, T. Trupke and M. A. Green, "Surface plasmon enhanced silicon solar cells," *J. Appl. Phys.* **101**, 093105 (2007).
5. W. L. Barnes, A. Dereux and T. W. Ebbesen, "Surface plasmon subwavelength optics," *Nature* **424**, 824 (2003).
6. F. Bohren and D. R. Huffman, *Absorption and Scattering of Light by Small Particles* (Wiley-Interscience, New York, 1983).
7. P. Spinelli, V. E. Ferry, J. van de Groep, M. van Lare, M. A. Verschuuren, R. E. I. Schropp, H. A. Atwater and A. Polman, "Plasmonic light trapping in thin-film Si solar cells," *J. Opt.* **14**, 024002 (2012).
8. L. Chen, W.C.H. Choy, and W.E.I. Sha, "Broadband absorption enhancement of organic solar cells with interstitial lattice patterned metal nanoparticles," *Appl. Phys. Lett.* **102**, 251112 (2013).
9. S. Pillai, F.J. Beck, K.R. Catchpole, Z. Ouyang, and M.A. Green, "The effect of dielectric spacer thickness on surface plasmon enhanced solar cells for front and rear side depositions," *J. Appl. Phys.* **109**, 073105 (2011).
10. H. Choi, J.P. Lee, S.J. Ko, J.W. Jung, H. Park, S. Yoo, O. Park, J.R. Jeong, S. Park, and J.Y. Kim, "Multipositional Silica-Coated Silver Nanoparticles for High-Performance Polymer Solar Cells," *Nano Lett.* **13**, 2204 (2013).
11. C.-I. Ho, D.-J. Yeh, V.-C. Su, C.-H. Yang, P.-C. Yang, M.-Y. Pu, C.-H. Kuan, I. C. Cheng, and S.-C. Lee, "Plasmonic multilayer nanoparticles enhanced photocurrent in thin film hydrogenated amorphous silicon solar cells," *J. Appl. Phys.* **112**, 023113 (2012).
12. Y. Shi, X. Wang, W. Liu, T. Yang, R. Xu and F. Yang, "Multilayer silver nanoparticles for light trapping in thin film solar cells," *J. Appl. Phys.* **113**, 176101 (2013).
13. M.A. Sefunc, A.K. Okyay, and H.V. Demir, "Volumetric plasmonic resonator architecture for thin-film solar cells," *Appl. Phys. Lett.* **98**, 093117 (2011).

14. A. Lin, S.-M Fu, Y.-K Chung, S.-Y Lai and C.-W Tseng, "An optimized surface plasmon photovoltaic structure using energy transfer between discrete nano-particles," *Opt. Lett.* **21**, 131 (2013).
15. R. Santbergen, R. Liang, M. Zeman, "A-Si: H solar cells with embedded silver nanoparticles," in *Photovoltaic Specialists Conference (PVSC)*, 2010, pp. 748.
16. M. Xue, L. Li, B.J.T. de Villers, H. Shen, J. Zhu, Z. Yu, A.Z. Stieg, Q. Pei, B.J. Schwartz and K.L. Wang, "Charge-carrier dynamics in hybrid plasmonic organic solar cells with Ag nanoparticles," *Appl. Phys. Lett.* **98**, 253302 (2011).
17. V. Santhanam, R.P. Andres, "Microcontact printing of uniform nanoparticle arrays," *Nano Lett.* **4** 41 (2004).
18. U. Kreibig, M. Vollme, *Optical properties of metal clusters* (Springer-Verlag, Berlin, 1995).
19. S. Zeng, K.-T. Yong, I. Roy, X.-Q. Dinh, X. Yu, F. Luan, "A review on functionalized gold nanoparticles for biosensing applications," *Plasmonics* **6**, 491 (2011).
20. S. A. Maier, H. A. Atwater, "Plasmonics: Localization and guiding of electromagnetic energy in metal/dielectric structures," *J. Appl. Phys.* **98**, 011101 (2005).
21. M. Meier and A. Wokaun, "Enhanced fields on large metal particles: dynamic depolarization," *Opt. Express* **8**, 581 (1983).
22. J. P. Kottmann and O. J. F. Martin, "Retardation-induced plasmon resonances in coupled nanoparticles," *Opt. Lett.* **26**, 1096 (2001).
23. C. Dahmen, B. Schmidt and G. von Plessen, "Radiation Damping in Metal Nanoparticle Pairs," *Nano Lett.* **7**, 318 (2007).
24. G. Xu, M. Tazawa, P. Jin, S. Nakao, and K. Yoshimura, "Wavelength tuning of surface plasmon resonance using dielectric layers on silver island films," *Appl. Phys. Lett.* **82**, 3811 (2003).
25. B. Hecht, H. Bielefeldt, L. Novotny, Y. Inouye, and D. W. Pohl, "Local Excitation, Scattering, and Interference of Surface Plasmons," *Phys. Rev. Lett.* **77**, 1889 (1996).
26. A. Webster and F. Vollmer, "Interference of conically scattered light in surface plasmon resonance," *Opt. Lett.* **38**, 244 (2013).
27. Z.-W. Liu, Q.-H. Wei, and X. Zhang, "Surface Plasmon Interference Nanolithography," *Nano Lett.* **5**, 957 (2005).
28. X. Deng, and E. A. Schiff, *Amorphous Silicon Based Solar Cells* (John Wiley & Sons, Ltd, 2005).
29. Y. A. Akimov, W. S. Koh and K. Ostrikov, "Enhancement of optical absorption in thin-film solar cells through the excitation of higher-order nanoparticle plasmon modes," *Opt. Exp.* **17**, 10195 (2009).
30. <http://www.spectra.com/sopra.html>.
31. A. Mandal and P. Chaudhuri, "Controlling the absorption spectrum within a thin amorphous silicon layer by using the size dependent plasmonic behaviour of silver nanoparticles," *J. Renewable Sustainable Energy* **5**, 031614 (2013).
32. S. H. Lim, W. Mar, P. Matheu, D. Derkacs, and E. T. Yu, "Photocurrent spectroscopy of optical absorption enhancement in silicon photodiodes via scattering from surface plasmon polaritons in gold nanoparticles," *J. Appl. Phys.* **101**, 104309 (2007).
33. D. F. Swinehart, "The Beer-Lambert Law," *J. Chem. Educ.* **39**, 333 (1962).
34. C. Noguez, "Surface Plasmons on Metal Nanoparticles: The Influence of Shape and Physical Environment," *J. Phys. Chem. C* **111**, 3806 (2007).
35. M. Meier, A. Wokaun, "Enhanced fields on large metal particles: dynamic depolarization," *Opt. Lett.* **8**, 581 (1983).
36. C. Noguez, "Optical properties of isolated and supported metal nanoparticles," *Opt. Mat.* **27**, 1204 (2005).
37. A. J. Haes, S. L. Zou, G. C. Schatz, R. P. Van Duyne, "Nanoscale Optical Biosensor: Short Range Distance Dependence of the Localized Surface Plasmon Resonance of Noble Metal Nanoparticles," *J. Phys. Chem. B* **108**, 6961 (2004).
38. P. Hanarp, M. Kall, D. S. Sutherland, "Optical Properties of Short Range Ordered Arrays of Nanometer Gold Disks Prepared by Colloidal Lithography," *J. Phys. Chem. B* **107**, 5768 (2003).
39. T. R. Jensen, M. D. Malinsky, C. L. Haynes, R. P. Van Duyne, "Nanosphere Lithography: Tunable Localized Surface Plasmon Resonance Spectra of Silver Nanoparticles," *J. Phys. Chem. B* **104**, 10549 (2000).
40. J. Robinson and Y. Rahmat-Samii, "Particle swarm optimization in electromagnetics," *IEEE Trans. Antennas and Propagat.* **52**, 397 (2004).
41. R. A. Pala, J. White, E. Barnard, J. Liu, and M. L. Brongersma, Design of Plasmonic Thin-Film Solar Cells with Broadband Absorption Enhancements, *Adv. Mater.*, **21**, 3504 (2009).

1. Introduction

Thin film solar cells have become a potential alternative to traditional crystalline silicon solar cells due to lower manufacturing costs, better flexibility, durability and shorter energy payback period. A better understanding of the underlying physics and the availability of mature fabrication technology makes amorphous silicon the preferred choice for thin film photovoltaic

cells. But the widespread adoption of thin film solar cells is limited by its relatively poor absorption efficiency owing to the indirect band gap of silicon [1]. In general, the efficiency of solar cells can be improved either by increasing the light absorption efficiency or by increasing the minority carrier life time. In order to increase the light absorption, it becomes necessary to incorporate light trapping mechanisms in solar cells. Recent advancements in the field of plasmonics have opened up the possibility of using metallic nanoparticles to increase the absorption of thin film solar cells [1–3]. Nanoparticles exhibit the phenomenon of surface plasmon resonance when illuminated with light of suitable frequency [4, 5]. Near the plasmon resonance frequency, metallic nanoparticles strongly scatter light incident on it. This scattering effect is the result of the collective oscillations of electrons to re-radiate electromagnetic radiation [6]. When placed on the surface of silicon substrate, metallic nanoparticles scatter light preferentially into it due to the high refractive index of silicon [7]. The particles also scatter the incident light at an angle, thereby increasing the path length of photons within the silicon substrate. As a result, the optical thickness of the active region increases, thereby allowing the semiconductor substrate to absorb higher levels of electromagnetic radiation [1].

Researchers have explored the possibility of placing nanoparticles on the surface [3, 4, 8], rear [9] and within the active region [10] of thin film solar cells. Multiple arrays of nanostructures placed either on the front, rear or both are used to further enhance the absorption efficiency [11–13]. The phenomenon of energy transfer between discrete nano-structures located at the surface and active region of a solar cell is used to control the flow of energy and improve absorption efficiency [14]. In these cases, enhancing the quantum efficiency has been considered over limited bands of wavelengths. Also, a loss in performance is possible if the metallic nanoparticles are introduced in the bulk [15, 16]. However, it is possible to prevent the metallic nanoparticles from acting as recombination centers either by using room temperature processes such as microcontact printing [17] or by passivating it with a dielectric coating [10]. Motivated by these facts, in this paper, we enhance the light absorption efficiency of a thin film a-Si solar cell by placing periodic arrays of silver nanoparticles at the surface and within the active region of the cell. The surface and bulk layer of nanoparticles enhances the absorption of lower and higher wavelengths respectively. In addition the absorption of light inside the substrate is further enhanced by the constructive interference of plasmon coupled light from surface and bulk nanoparticle layers.

2. Background theory

Understanding the basic mechanism of localized surface plasmon resonance and various parameters affecting it is necessary to engineer the nanoparticles for light trapping applications in solar cells. The resonant behavior of localized surface plasmons are restricted to a limited range of frequencies determined by the size and shape of the particles, dielectric functions of the involved media, and the electromagnetic interaction between them [18]. When the frequency of light incident on the nanoparticles match the natural frequency of the oscillating surface electrons, the phenomenon of surface plasmon resonance is established [19]. The collective response of the electrons in spherical metallic nanoparticles with dimension much lesser than the wavelength of light is described by the dipolar polarizability α ; [20]

$$\alpha = 3V \left(\frac{\epsilon - \epsilon_m}{\epsilon + 2\epsilon_m} \right) \quad (1)$$

where V is the particle volume, ϵ_m is the dielectric function of the embedding medium and ϵ is the dielectric function of the metallic nanoparticle. The size dependent dielectric function the particle $\epsilon(\omega, D)$ is given by, [18]

$$\varepsilon(\omega, D) = \varepsilon_{IB} + \left(1 - \frac{\omega_p^2}{\omega^2 + i\omega\gamma(D)} \right) \quad (2)$$

where D is the diameter of the particle and $i = \sqrt{-1}$. The size independent first term ε_{IB} is due to interband transitions. The second term is the Drude-Sommerfeld free electron term which contains the bulk plasmon frequency ω_p , given by $\omega_p^2 = Ne^2/m\varepsilon_0$ where N is the density of free electrons, e is the electronic charge, m is the effective mass of an electron and ε_0 is the free-space dielectric constant, and the size-dependent damping constant γ ; [18]

$$\gamma(D) = \gamma_0 + 2 \left(\frac{Av_F}{D} \right) \quad (3)$$

where γ_0 is the bulk damping rate and v_F is the Fermi velocity of the electrons. A is a dimensionless size parameter which accounts for the additional surface damping terms, such as the inelastic collisions between electrons and chemical interface damping. Inelastic collisions shorten the mean free path of the electrons when nanoparticle size decreases. Chemical interface damping occurs in embedded nanoparticles, where the fast energy transfer between the particle and its surroundings results in the loss of phase coherence of the collective electron oscillation.

The particle polarizability becomes large when $\varepsilon = -2\varepsilon_m$, and this effect is called surface plasmon resonance. At resonance the particle scattering cross-section area, C_{scat} , a parameter that determines the extent to which scattering of light occurs, is several times the geometric cross section of the particle [6].

$$C_{scat} = \frac{1}{6\pi} \left(\frac{2\pi}{\lambda} \right)^4 |\alpha|^2 \quad (4)$$

where λ is the wavelength of the incident light. For particles with diameter in the range of a few nanometers, scattering is also accompanied by absorption. As particle diameter increases to around 100 nanometers, the scattering effect strongly outweighs the absorption by the particle [2]. Also, the resonance is accompanied by another process, namely dynamic depolarization [21]. As size increases, the oscillation of the conduction electrons at resonance goes out of phase, resulting in a red shift of the particle resonance. The increase in size also results in higher radiation damping, which results in the broadening of the range of frequencies at which resonance occurs [22, 23]. The surface plasmon resonance can be tuned to a larger extent either by overcoating or sandwiching the nanostructure with a dielectric medium. The medium can markedly enhance the red shift of the central wavelength and consequently obtain a wide tunable range at higher wavelengths [24]. Both red shifting and broadening of resonance frequencies are advantageous for the solar cell [2].

The surface plasmon waves from multiple resonating structures can interfere with each other and produce interference patterns [5, 25–27]. This phenomena is used for field patterning in nanophotolithography techniques [27]. The phenomenon of surface plasmon wave interference from resonating nanostructures can be used to enhance the electric field inside an absorber layer sandwiched between the structures, which in turn results in higher levels of absorption within the layer. Due to the multiple and high-angle scattering from both the layers of nanoparticles, the effective optical path length of light increases inside the cell. This results in several fold increase in the optical thickness while the physical thickness remains constant [1].

3. Proposed Solar Cell Design

In our thin film solar cell design, the active region is made of amorphous silicon having a thickness of $0.5 \mu\text{m}$. Spherically shaped silver nanoparticles are placed periodically in rectangular arrays on the surface as well as inside the active region of the substrate. Particle layers are placed in such a way that nanoparticles in both layers are vertically aligned. The perspective view of the design described above is shown in Fig. 1(a). The schematic diagram in Fig. 1(b) shows the various parameters of the proposed design. The radius of the nanoparticles on the surface and in the active region are denoted by R_s and R_b respectively. The period of the nanoparticle array is denoted by P and the distance from the surface of the solar cell to the top of the bulk array is denoted by T .

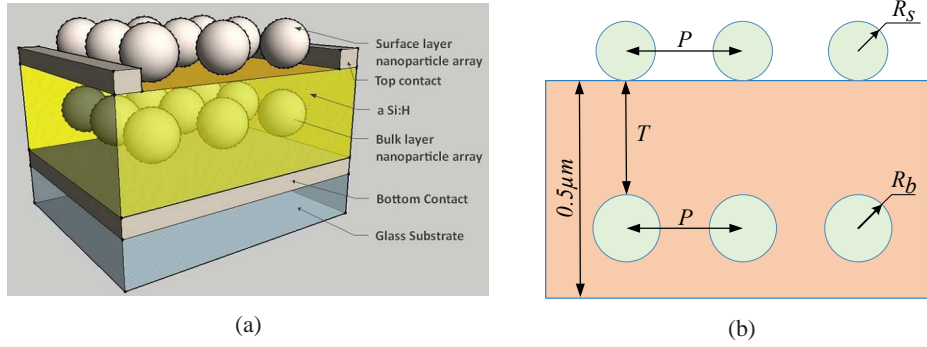


Fig. 1: (a) Perspective view of the solar cell with silver nanoparticle arrays on the surface and in the bulk.(b) Various parameters of the considered design.

The device performance is compared with a few existing reference designs to understand the improvement in absorption efficiency. A $0.5 \mu\text{m}$ thick active region of amorphous silicon is considered for all designs. The relatively thicker absorber layer is taken in order to absorb light of higher wavelengths [28] and also to compensate for the loss in volume of the active region due to the incorporation nanoparticles inside the a-Si substrate. Design 1, considered as the primary reference, contains only the a-Si layer and does not incorporate any nanoparticle arrays for light trapping. Design 2 contains silver nanoparticle arrays on the surface, similar to the design in [29]. A silver nanoparticle array is introduced into the bulk of the amorphous silicon active region in Design 3. Design 4 corresponds to the proposed structure where nanoparticle arrays are introduced at both the surface and bulk of the silicon layer. Initially the radii of the nanoparticles on the surface (R_s) and in the active region (R_b) are chosen as 50 nm and 70 nm respectively. The purpose is to exploit the plasmonic enhancement provided by different layers at different wavelength regimes so as to enhance the absorption over a wide band of wavelengths. The nanoparticles on the surface resonates at lower wavelengths and provides plasmonic enhancement in these regions. On the other hand the particle layer in the bulk with nanoparticles of higher size resonates at higher wavelengths and provide plasmonic enhancement in these wavelengths. In order to allow horizontal and vertical coupling of light between the nanoparticles, the period of the nanoparticle arrays (P) is taken as 200 nm and the distance from the surface of the solar cell to the top of the bulk array (T) is taken as 280 nm . These parameters are optimized in a later section to find out the best possible configuration that gives the maximum absorption enhancement. The initial specifications of the nanoparticle arrays for designs 2 to 4 are summarized in Table 1.

The three dimensional finite difference time domain analysis (FDTD) tool provided by

Table 1: Specifications for the proposed design and reference designs (all dimensions are in nm)

Design	R_s	R_b	P	T
Design 1	-	-	-	-
Design 2	50	-	200	-
Design 3	-	70	200	280
Design 4	50	70	200	280

Lumerical is used for the design simulation. The amorphous silicon material is optically modeled using the refractive index data provided in the SOPRA N&K Database, a widely cited and verified experimental database of various materials [30]. A normally incident plane wave source of unit amplitude with a wavelength range from 400 nm to 1100 nm is placed above the surface nanoparticle layer. Periodic boundary conditions are used for the side boundaries to model the periodic nature of the particles. The Perfectly Matched Layer (PML) boundary conditions are used for upper and lower boundary to approximate the effect of infinite space and substrate respectively. The reflecting bottom contact is neglected in order to allow only a single pass of the incoming light [31]. This provides the absorption enhancement solely due to the nanoparticles [32] and confirms that any enhancement in light absorption is only due to the incorporation of nanoparticles, not by the anti reflecting front or reflecting back contacts. Mesh size of 2 nm is used for the regions where the particles are present and 3 nm for the a-Si absorber region. The absorbed power within the active region of the solar cell is calculated with the help of 3-D power monitors placed on the entire a-Si substrate. The monitors record field data over the entire volume of the substrate and find the power absorbed as a function of space. For the design with particles embedded in the bulk, the power absorbed by the particles has to be deducted from the net absorbed power, since it does not contribute to the electron-hole pair generation. The power absorbed by the silicon absorber layer is calculated by applying a spatial filter which integrate the absorption within the filter region (here the a-Si substrate). The quantum efficiency and total quantum efficiency are calculated for all the designs considered [12].

The quantum efficiency of a solar cell for a particular wavelength, $QE(\lambda)$, is defined as the ratio of the absorbed power within the solar cell, $P_{abs}(\lambda)$, to the incident power of light, $P_{in}(\lambda)$;

$$QE(\lambda) = \frac{P_{abs}(\lambda)}{P_{in}(\lambda)}. \quad (5)$$

The quantum efficiency of all designs in Table 1 are compared in Fig. 2 to understand the absorption efficiency at different wavelengths.

It can be observed from Fig. 2 that the absorption efficiency of amorphous silicon (Design 1) drops drastically for wavelengths above 800 nm . The introduction of nanoparticles on the surface improves the absorption efficiency of a-Si for a range of wavelengths between 400 nm and 750 nm , but causes little improvement at higher wavelengths. On the other hand, the introduction of nanoparticles inside the active region results in significant improvement in the absorption efficiency at wavelengths above 850 nm , even though it has minimal effect at lower wavelengths. The proposed design exploits the absorption enhancement caused by both layers and produces improved absorption at all wavelengths. Around 800 nm , the simultaneous resonance from particles in both the layers enhances the field in the active region sandwiched between the layers. The inter-layer particle interaction produces an improvement in photon absorption when compared to the enhancements caused by individual layers. The field profile

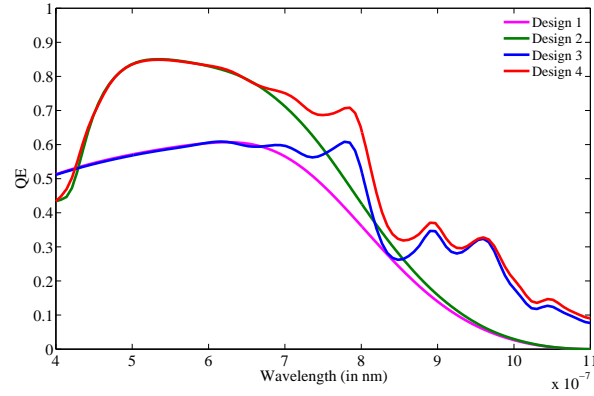


Fig. 2: Quantum efficiency of various designs under consideration as a function of wavelength of light.

inside the amorphous silicon substrate at various wavelengths is given in Fig. 3.

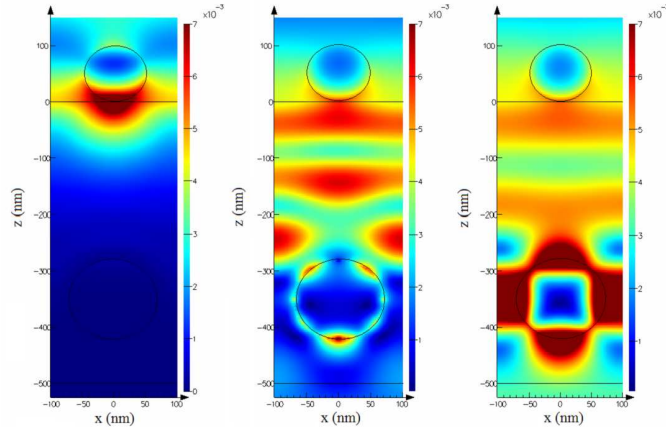


Fig. 3: Field profile at different wavelengths inside the amorphous silicon substrate of Design 4. (a),(b) and (c) correspond to wavelengths 526 nm, 792 nm and 1072 nm respectively.

It is evident from Fig. 3(a) that the high energy radiation is absorbed near the surface and fails to penetrate enough into the substrate so as to resonate the nanoparticles buried inside the amorphous silicon. At higher wavelengths, silicon has poor absorption, as a result of which the incident radiation penetrates deep into the substrate, as seen in Fig. 3(c). This is in accordance with Beer-Lambert's Law, which states that the extent of absorption in a solid depends inversely on the wavelength of the incident radiation [33]. In order to enhance the light absorption in lower wavelengths, particles with a surface plasmon resonance frequency falling in this wavelength region are placed on the surface of the active region. Larger particles are employed in the active region of the substrate for providing the plasmonic enhancement at higher wavelengths, since an increase in particle size and embedding dielectric medium causes a red shift in the resonance frequency. The radii of particles in both the layers are chosen in such a way that their resonance frequency does not fall in very low or very high frequencies. This is done so

as to exploit the enhancement due simultaneous resonance from both the nanoparticle layers at intermediate wavelengths. In the intermediate wavelengths, the particles in both layers strongly scatters of light which interfere constructively in the silicon region sandwiched between them. The constructive light wave interference results in a high intensity field pattern in the mid region between the particle layers, seen in Fig. 3(b), thereby enhancing the absorption at these wavelengths.

For the broad spectrum of incident electromagnetic radiation, the total quantum efficiency, TQE , which takes the solar spectral irradiance into account, determines the overall performance of the solar cell. TQE is the fraction of incident photons that are absorbed by the solar cell.

$$TQE = \frac{\int_{\lambda_1}^{\lambda_2} \frac{\lambda}{hc} QE(\lambda) I_{AM1.5}(\lambda) d\lambda}{\int_{\lambda_1}^{\lambda_2} \frac{\lambda}{hc} I_{AM1.5}(\lambda) d\lambda} \quad (6)$$

where h is Planks constant, c is the speed of light in the free space and $I_{AM1.5}$ is the AM 1.5 solar spectrum. TQE and absorption enhancement for the broad spectrum of light as compared to the plain reference silicon solar cell are listed in Table 2.

Table 2: Comparison of TQE of the proposed design with the other considered designs and their enhancement as compared to a-Si without nanoparticles

Design	TQE (%)	enhancement
Design 1	38.61	1.0000
Design 2	49.91	1.2926
Design 3	45.08	1.1675
Design 4	56.01	1.4507

The absorption enhancement over the entire wavelength region translates to a higher TQE for Design 4 when compared to the other considered designs. A TQE of 56.01% is obtained for the proposed design.

4. Variation of absorption efficiency with design parameters

There are various parameters of the proposed design that influence the absorption profile of thin film substrate. Change in nanoparticle radius shifts the surface plasmon resonance frequency whereas the mutual interaction between the nanoparticle layers is affected by a change in particle layer separation as well as the alignment of particles in both the arrays. The effect of these parameters towards the absorption efficiency of the solar cell is studied in detail.

4.1. Influence of particle layer separation in absorption efficiency

The variation in absorption efficiency ($QE(\lambda)$) with change in inter particle layer separation (T) is investigated first. T is varied from 36 nm to 360 nm while keeping the period of both nanoparticle arrays at 200 nm and radii of nanoparticles in surface and bulk layer at 50 nm and 70 nm respectively (same as in design 4). $QE(\lambda)$ and TQE for various inter layer separations is given in Fig. 4(a) and Fig. 4(b) respectively.

Figure 4(a) shows that below 750 nm wavelength, the QE is almost the same for all values of T . A slight variation in QE is seen only when the bulk layer lies close to the surface (at $T = 36$ nm). In the lower wavelength regions, only the surface layer is responsible for the absorption enhancement. When the bulk layer is located close to the surface, it reduces the

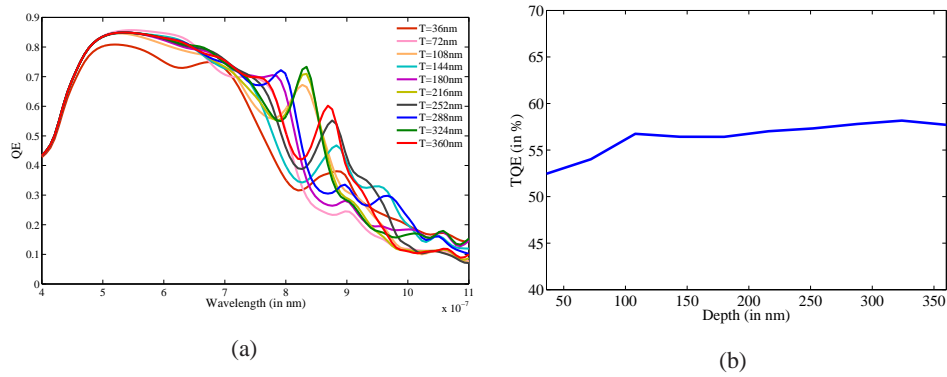


Fig. 4: Variation of QE and TQE with change in inter particle layer separation

enhancement caused by the surface layer. The bulk layer occupies the region where the field is intensified due to the surface layer and reduces the absorption by the active region. For wavelengths ranging from 750 nm to 950 nm , a sharp peak in absorption is observed when T is increased beyond 108 nm . This peak in absorption is attributed to the constructive interference of plasmon coupled light between the two nanoparticle layers. The particles in both layers resonates in this wavelength region and collectively contributes to the absorption enhancement. At higher wavelengths the nanoparticles in the bulk layer resonate and contributes towards the absorption enhancement. The enhancement varies significantly with change in T . The combined effect of plasmonic enhancement from individual nanoparticle layers and field enhancement due to light wave interference determines the TQE of the device. The TQE for different particle layer separations is shown in Fig. 4(b). The net absorption increases with an increase in the depth at which the bulk layer is buried. The maximum absorption occurs when the bulk layer is located at a distance of 324 nm below the surface.

The wavelength at which the peak in absorption due to constructive interference of light waves occur, (λ_{int}), varies with change in particle layer separation (T) and is given in Fig. 5(a).

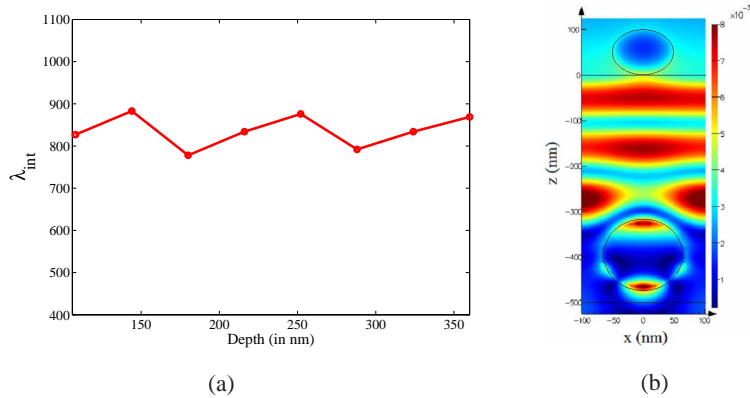


Fig. 5: (a) Variation of wavelength at which interference occurs with nanoparticle layer separation (b) Field profile at wavelength 834 nm for an inter layer separation of 324 nm

It is observed from Fig. 5(a) that λ_{int} shows a periodic trend with increase in inter layer

separation (T). The value of λ_{int} is limited between 770 nm and 870 nm and repeats periodically for an inter particle layer separation of around 111 nm . The field intensity distribution inside the a-Si substrate due to interference for an inter layer distance of 324 nm is shown in Fig. 5(b).

4.2. Influence of particle radii in absorption efficiency

The size of silver nanoparticles in both surface and bulk layer influences the absorption inside sandwiched a-Si substrate. The variation in absorption efficiency of the design with change in nanoparticle radii of surface layer (R_s) and bulk layer (R_b) is studied separately. R_s is varied from 0 to 100 nm while keeping the other design parameters same as that of Design 4. Similarly R_b is also varied from 0 to 100 nm with other parameters kept at the same value as in Design 4. The variation of $QE(\lambda)$ with R_s and R_b are shown in Fig. 6(a) and Fig. 6(b) respectively.

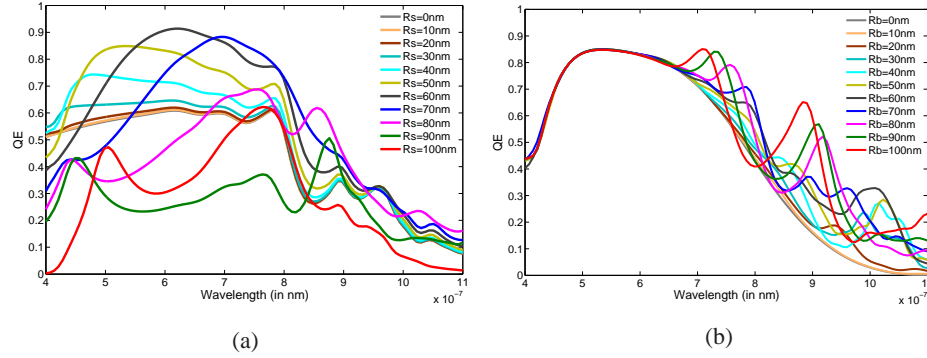


Fig. 6: Variation of QE with wavelength for different (a) surface and (b) bulk layer particle radii.

Figure 6(a) shows that at wavelengths below 800 nm the absorption peak shifts towards the right with increase in R_s . The magnitude of the absorption peak increases when the R_s increases from 0 to 70 nm . Further increase in R_s results in the reduction of magnitude of absorption peak in this wavelength region. Another peak in QE begins to appear at lower wavelengths around $400 - 550\text{ nm}$ range for R_s values higher than 70 nm . It is also observed that the QE curve broadens as R_s increases.

The red-shift and broadening of QE with increase in R_s is because of dynamic depolarization and radiation damping [21–23]. The field experienced by the nanoparticles can be considered as spatially constant but with time varying phase when the size of the homogeneous particle is much smaller than the wavelength of the incident light. This is known as the quasistatic limit [34]. For smaller values of R_s the displacement of charges is homogeneous which result in a dipolar charge distribution on the surface. These charges give rise to only one proper resonance [34]. As R_s increases, the displacement of electronic cloud loses its homogeneity. As a result of this multipolar charge distributions are induced [18]. In addition to this, an additional polarization field is produced by the accelerated electrons [35]. This field reacts against the quasistatic polarization field and shifts the position of the resonant modes to larger wavelengths. Also the electrons lose energy due to this secondary radiation and experience a damping effect which results in the widening of the range of frequencies over which surface plasmon resonance occurs [36]. Thus the increase in particle size makes broader and asymmetric surface plasmon resonance peaks which are red-shifted and reduced in intensity.

Figure 6(b) shows that the particles in the bulk layer do not affect the absorption at lower wavelengths but have significant effect at higher wavelengths. The frequencies and intensities of localized surface plasmon resonances are known to be sensitive to the dielectric properties

of the medium [37–39] and in particular, to the refractive index of matter close to the particle surface [37,39]. The larger particles show better absorption enhancement at higher wavelengths. Two distinct absorption peaks are observed for bulk layer nanoparticles with R_b above 70 nm. An increase in the particle radii gives the absorption peak with higher QE . The effect of varying nanoparticle radii of bulk and surface layer towards the absorption of photons over the entire spectrum is shown in Fig. 7.

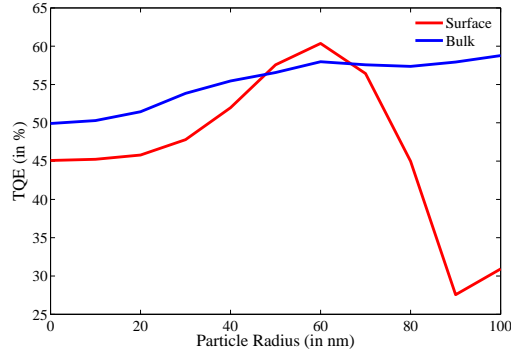


Fig. 7: Variation in TQE with change in surface and bulk layer nanoparticle radii

It is evident from the graph that the surface layer radius variation affects the absorption to a higher extend. TQE increases with increase in R_b . An initial increase in the radius of the surface layer nanoparticles causes an increment in TQE but decreases when the particle radii exceeds 60 nm.

4.3. Influence of vertical alignment of particle layers

The proposed design contains vertically aligned nanoparticle arrays in the surface as well as in the bulk of the a-Si substrate. But perfect vertical alignment is difficult to attain practically. In order to understand the extend to which the alignment of two nanoparticle layers affect the light absorption in the proposed design, the bulk array is moved in the horizontal direction while keeping the position of the surface array unaltered as shown in Fig. 8. The horizontal distance l between the centers of nanoparticles in both the layers is a measure of misalignment between the particle layers. The variation in absorption when the bulk array is moved away from the normal is shown in Fig. 9.

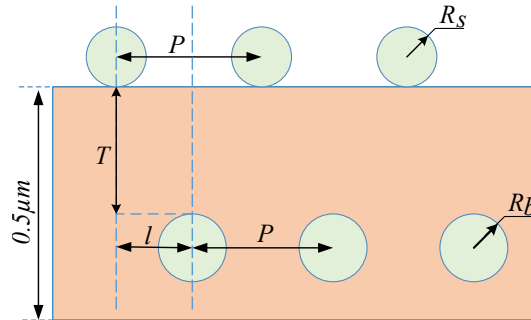


Fig. 8: Alignment of particles in bulk and surface array.

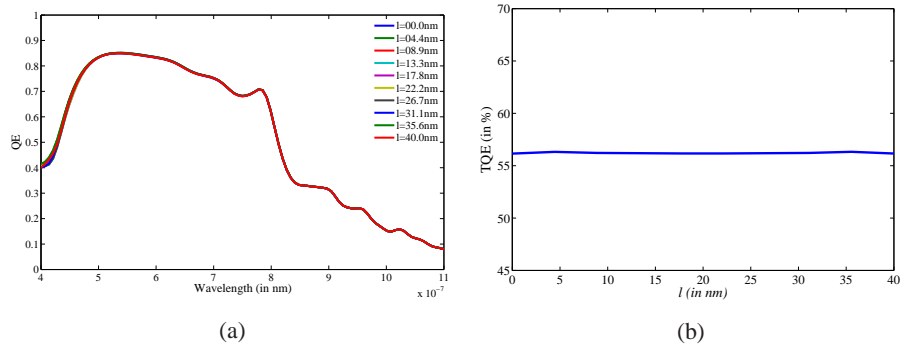


Fig. 9: Variation of QE and TQE with change in the alignment of particles.

The QE and TQE plot for various l values shows that there is very little change in absorption efficiency when the nanoparticles in the bulk array is moved horizontally away from the normal passing through the center of the top layer nanoparticles. A slight mismatch in vertical alignment of nanoparticle arrays does not affect the overall absorption. Therefore the constraint of perfect vertical alignment can be relaxed while placing nanoparticle arrays in the solar cell.

5. Optimization of design parameters

The performance of the solar cell can be improved by tuning the parameters of the cell, namely the radii of the nanoparticles in both arrays (R_s, R_b), the period of the rectangular array of particles (P) and the vertical distance between the two particle layers (T). The optimization is carried out using the Particle swarm optimization algorithm which converges to an optimum set of design parameters after a certain number of iterations [40]. An a-Si active region of thickness $0.5 \mu m$ is considered for the solar cell. Values between $5 nm$ and $100 nm$ were considered for R_s and R_b . The period, P , was considered from the minimum possible value, equal to the diameter of the larger particle among surface and bulk layer, to a maximum value of $600 nm$. The value of T is varied from zero to a maximum possible value equal to the difference between the thickness of the active region and diameter of bulk layer particle.

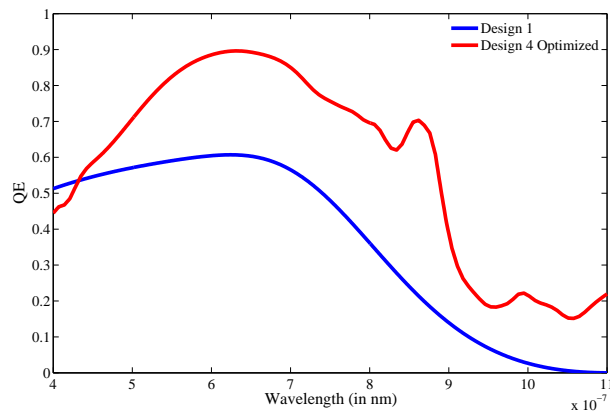


Fig. 10: QE variation with wavelength for Design-1 and optimized Design 4

For the proposed solar cell design (Design 4), the optimal radii for the surface and bulk layer particles are found to be 66.4 nm and 84.6 nm respectively. A period of 242.3 nm is obtained for the optimized design. A distance of 405.9 nm from the surface of the solar cell to the center of the bulk layer is found to be optimal for a solar cell. The optimized design resulted in a TQE of 62.33% which is 1.61 times higher than the plain reference a-Si solar cell. This translates to an efficiency enhancement of 61.44% . The quantum efficiency of the optimized design is compared with plain a-Si substrate in Fig. 10. The absorption efficiency of the substrate is improved for all wavelengths ranging from 450 nm to 1100 nm in the proposed design.

6. Discussions and Conclusion

The proposed solar cell design exploits the cumulative plasmonic enhancement from different nanoparticle layers at different wavelengths and improves the absorption efficiency over the entire range of wavelength. The front and back contacts which were neglected purposefully in the study can further improve the absorption efficiency of the proposed design. The effect of including contacts toward the overall absorption efficiency enhancement was investigated. Design 4 is optimized by incorporating the front and back contacts. A 20 nm thick ITO (Indium tin oxide) front contact is considered in between the surface nanoparticle layer and a-Si substrate and $1.5\text{ }\mu\text{m}$ thick Al back contact is considered in the rear side of the active region. Nanoparticle layer parameters are optimized using the Particle swarm algorithm which result in a TQE of 65.37% . This is 1.4 times higher than the corresponding $0.5\text{ }\mu\text{m}$ thick plain a-Si solar cell with 20 nm front ITO anti reflection coating and $1.5\text{ }\mu\text{m}$ back Al contact. The slight improvement in TQE is due to the reflection of light at the bottom cell boundary by the Al contact and the anti reflection property of the front ITO contact.

For calculating the short circuit current, recombination occurring in the device need to be considered. Recombination due to nanoparticles can be mitigated either by depositing nanoparticles at room temperature or by coating the nanoparticles with a thin dielectric layer. We studied the effect of dielectric coating thickness on TQE and found that the variation is minimal if the thickness is below 3 nm . If the a-Si film thickness is thin, the recombination in the bulk of a-Si can be neglected [41]. Hence the enhancement in the short circuit current will be a replica of the enhancement in TQE .

In summary, the theoretical study shows that the thin film amorphous silicon solar cell with nanoparticle arrays placed on the surface and in the semiconductor layer showed significant improvement in absorption efficiency. The metallic nanoparticles at the surface contributes to the enhancement at lower wavelengths and those embedded within the absorber layer contributes to the enhancement at higher wavelengths. The constructive interference of plasmon coupled light from nanoparticle layers further enhances the field intensity at intermediate wavelengths. Therefore, the design put forward in this paper exploits the surface plasmon resonance from metallic nanoparticles at all wavelengths and thus provides significant improvement in the overall light absorption efficiency.

7. Acknowledgment

The authors would like to thank the anonymous reviewers for their valuable comments and suggestions to improve the quality of the paper.

